Development of microfluidic device and electronic infusion system to fabricate microfiber of alginate and carbon nanotube

Abdulsalam Ali Ahmed Salman, Chin Fhong Soon, Gim Pao Lim
Faculty of Electrical and Electronic Engineering, Universiti Tun Hussein Onn Malaysia, Parit Raja, Malaysia

Article Info

ABSTRACT

A novel microfluidic device and electronic infusion system for carbon nanotube-calcium chloride alginate microfibers are presented in this study. The microfluidic device was designed using Google SketchUp and 3D printing, and the electronic infusion system-controlled alginate solution flow to the calcium chloride jar—the silicon-PDMS microfluidic device produced calcium alginate microfibers with carbon nanotubes. The device to emulsify the two fluids was modeled in COMSOL Multiphysics. The microfluidic device and calcium chloride jar received juice from the syringe pump via a high-flow infusion pump (100, 150, and 200 rpms). Field emission scanning electron microscopes (FE-SEM), Fourier transform infrared spectroscopy (FTIR), Raman spectroscopy, and X-ray diffraction analysis (XRD) detected highly concentrated microfibers with sizes from 10 to 100 um. I-V characterization showed that sodium alginate's carbon nanotubes at 5%, 6%, and 7% produced fiber sizes between 16.6 and 30 ums. Compared to pure alginate microfibers, those with carbon nanotubes and calcium chloride had higher mechanical strength and electrical conductivity. This study shows that the developed system can produce advanced microfibers with improved properties for various applications.

Corresponding Author:

Chin Fhong Soon
Faculty of Electrical and Electronic Engineering, Universiti Tun Hussein Onn Malaysia
Parit Raja, Johor, Malaysia
Email: soon@uthm.edu.my

1. INTRODUCTION

The development of microfluidic devices and electronic infusion systems has gained considerable attention in recent years due to their diverse applications in biotechnology, drug delivery, and chemical—processing [1]. One potential application of microfluidic devices is microfiber fabrication, with a wide range of applications. These systems enable precise fluid flow control at the microscale, facilitating the manipulation of small volumes of fluids and integrating chemical and biological processes. Among the promising applications of microfluidic devices is the fabrication of microfibers, which find utility in tissue engineering, drug delivery, and filtration [2]. The combination of alginate and carbon nanotubes holds excellent potential for producing microfibers with enhanced mechanical properties and electrical conductivity [3].

The research presented here [4] adds to the growing knowledge in the microfiber fabrication field. It contributes to the ongoing efforts to develop efficient and scalable methods for producing conductive microfibers. Microfluidic devices have been widely studied for their potential applications in various fields, such as drug delivery, chemical synthesis, and biological analysis [5]. This [6] investigated the advancements of carbon nanomaterials for biomedical applications. The research highlights the promising potential of carbon nanotubes in various biomedical fields, paving the way for future developments in healthcare technologies. Mafroos *et al.* [7] demonstrated the successful implementation of a passively Q-switched erbium-doped fiber laser using

graphene and carbon nanotube saturable absorbers, showcasing the potential of these materials for enhancing laser performance; the findings contribute to advancements in laser technology and hold promise for various applications in photonics and telecommunications. Kurokawa *et al.* [8] demonstrated the enhanced conversion efficiency of dye-sensitized solar cells (DSSCs) using ozone-treated titanium dioxide (TiO2) photoanode and an optimized counter electrode composed of carbon nanotubes (CNT) and poly (diallyldimethylammonium chloride) or PDDA. The study's findings provide valuable insights into improving the performance of DSSCs and offer potential advancements in renewable energy technologies. A study in [9] presented a simulation of carbon nanotube field-effect transistors (CNTFETs) simulations of serious-k gate dielectrics. The simulations of CNTFETs using various high-k gate dielectrics. The study provides valuable insights into the performance of CNTFETs with different gate dielectric materials and offers potential avenues for enhancing the electrical characteristics of these devices [10].

The research offers valuable insights into the performance of CNTFETs with different gate dielectric materials and provides potential strategies for enhancing the device's electrical characteristics. The combination of carbon nanotubes (CNTs) and calcium chloride (CaCl2) is a promising material for fabricating microfibers due to the unique properties of CNTs and the crosslinking capabilities of $CaCl_2$ [11]. However, traditional methods for fabricating microfibers using CNTs and CaCl2 can be complex and time-consuming [12]. To address this issue, researchers have recently studied microfluidic devices and electronic infusion systems to simplify and automate the microfiber fabrication process [13].These systems are technology to fabricate microfluidic channels and reservoirs, and electronic infusion pumps to control the flow of materials through the channels [14]. One example of the microfluidic device and electronic infusion system for fabricating alginate microfibers of CNTs was described by [15]. Guo *et al.* [16] demonstrate the system's capability to fabricate microfibers with high yields and reproducibility. Guo *et al.* [17] also show that the microfibers produced by their system have improved mechanical properties compared to those using traditional methods. Generally, the development of microfluidic devices and electronic infusion systems has revolutionized the fabrication of alginate microfibers of CNTs and CaCl2, making the process simpler and more efficient. However, the fabrication of alginate and carbon nanotubes is limited by the difficulty in uniformly dispersing the carbon nanotubes within the alginate matrix [3]. To address this challenge, the use of calcium chloride as a crosslinking agent has been proposed as a means of import improve carbon nanotubes within the alginate matrix [18].

In this study, we present the developments of the microfluidics device and electronic infusion system for fabricating alginate and carbon nanotube microfibers. The microfluidic device was designed using Google SketchUp software and printed using the 3D printer. In contrast, the electronic infusion system was designed to control the flow of fluids and the addition of chemicals to the microfluidic. This research aims to show the feasibility of using the microfluidic device and electronic infusion system to fabrication of the alginate microfibers of carbon nanotubes and calcium chloride. To achieve this aim, we will investigate the effects of various process parameters on the properties of the resulting microfibers, including the flow rate of the fluids, the concentration of the chemicals, and the crosslinking time. Overall, the development of the microfluidic device and electronic infusion system for the fabrication of alginate microfibers with carbon nanotubes and calcium chloride has the potential to revolutionize the field of microfiber fabrication and provide a new platform for the integration of various chemical and biological processes at the microscale.

2. METHOD

This section outlines the methodology used to design and fabricate a microfluidic device for producing alginate and carbon nanotube microfibers, as illustrated in Figure 1. The design process involved using Google SketchUp and COMSOL Multiphysics for modeling and designing the microfluidic device. The 3D model was converted to STL format, printed as a physical mold, and used to create a polydimethylsiloxane (PDMS) microfluidic device through the PDMS molding process. Furthermore, the electronic development of the device was conducted, and the produced alginate microfibers were characterized using Fourier transform infrared spectroscopy (FTIR), Raman spectroscopy, and X-ray diffraction.

2.1. Design of the 3D mold

The design of the 3D mold using a flow chart involves several steps, as shown in Figure 2. Starting with conceptualization and planning, the mold is created using Google Sketchup 2021 and exported as an STL file. The file is then imported into slicing software, like Ultimaker Cura, to generate G-code instructions for the 3D printer. The printer reads the instructions and builds the object layer by layer, taking several hours to complete depending on the mold's size and complexity. After printing, any necessary post-processing is performed, and the final 3D mold is ready for use. It can be used repeatedly to create multiple copies with consistent quality and accuracy, making it a versatile and efficient solution for producing complex and customized objects.
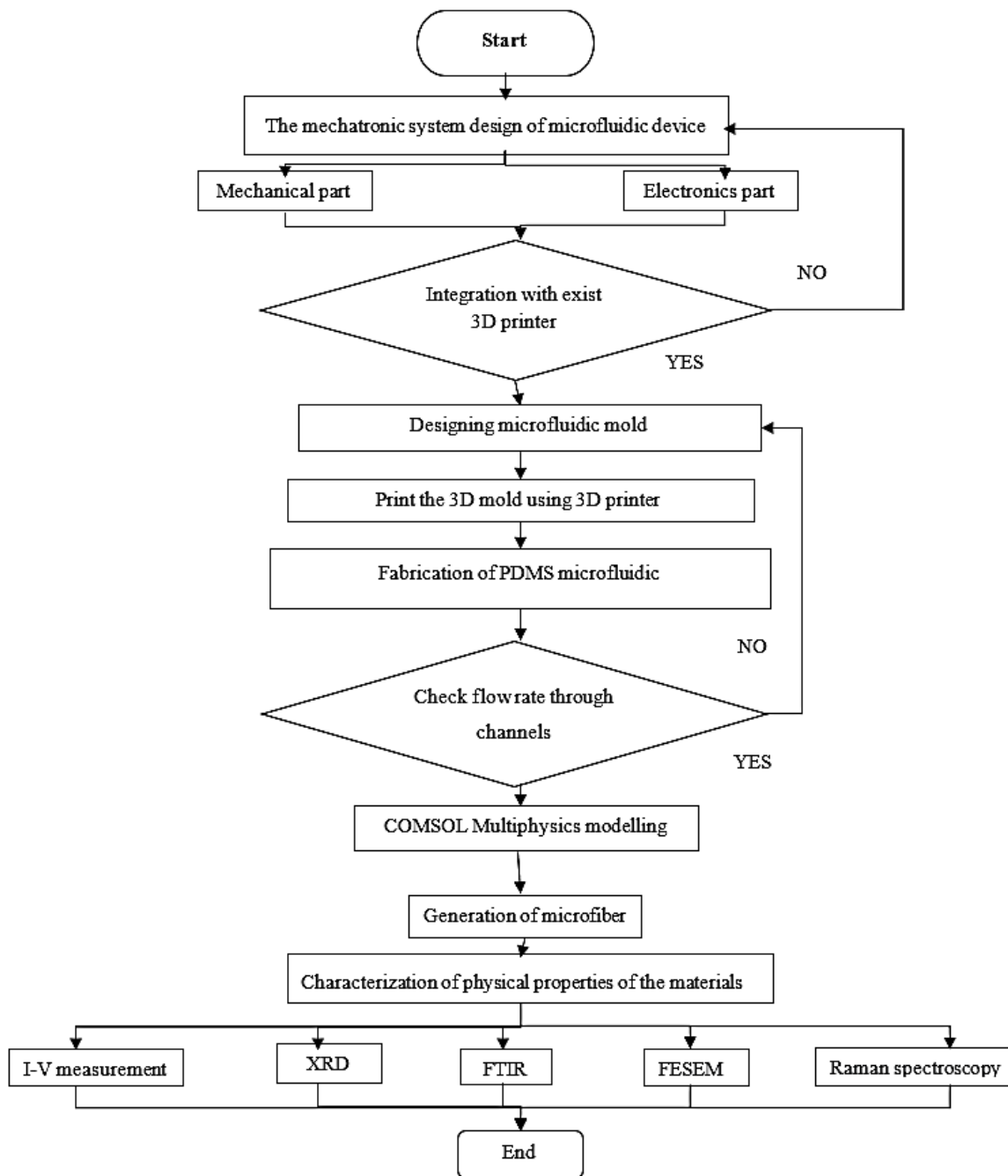
Figure 1. The flow chart of early project methodology

2.2. Fabrication of a microfluidic extrusion head

The fabricating of a microfluidic extrusion head involves several key steps, as outlined in Figure 3. First, a design for the device was created using Google SketchUp 2021 software, enabling a 3D model to be generated and used as a blueprint for the fabrication process. To make the device, a mixture of PDMS and silicon in a 10:1 ratio was chosen for its moldability and compatibility with microfluidic applications. The device was then fabricated according to its design specifications, which included dimensions such as length, width, height, radio for the inlet and outlet channels, and the interaction channel. The fabrication process included pouring the mixture into a mold that matched the dimensions specified in the design, And then curing the material. After removal from the mold, the channels were etched using a wet etching technique to ensure they were of the correct dimensions and had smooth surfaces. The final product was inspected for defects and tested to verify that it met the desired specifications before being ready for use in microfluidic experiments.
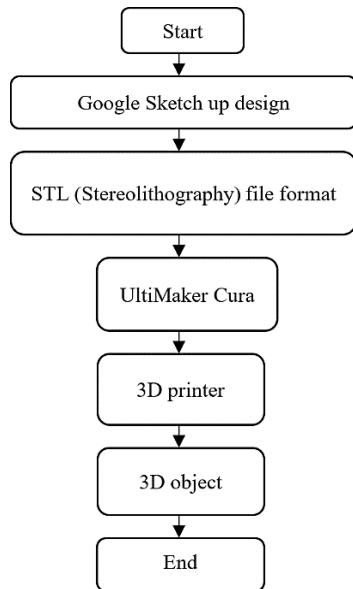
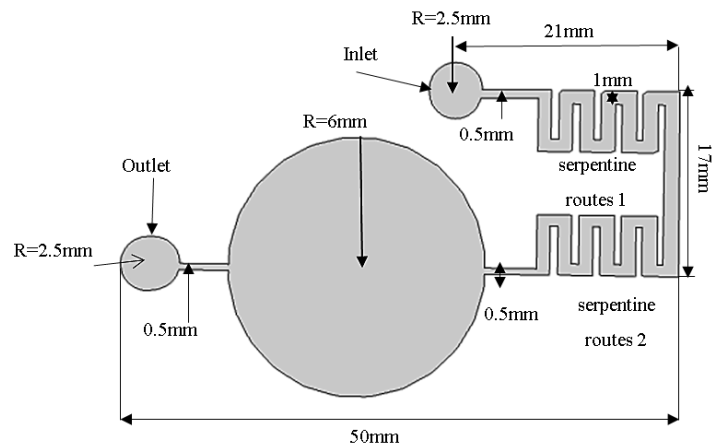Figure 2. Flowchart of the design of the 3D mold

Figure 3. The dimensions of microfluidic device design in millimeter (mm)

2.3. Simulation of the microfluidic

This study simulated a microfluidic system using COMSOL Multiphysics 5.6.0.280 to generate extrusion microfibers. The microfluidic device was designed in Google SketchUp 2021 and imported as a DXF file format into COMSOL Multiphysics. The fluid parameters were set to 1000 kg/m³ in density, and 1 Pa-s in dynamic viscosity, and a no-slip boundary condition was assumed due to the use of hydrophobic PDMS as the material for the microfluidic device. The mesh network was chosen with fine-sized elements to mimic highly fine meshing. The inlet was set to 0 mol/m^3 as a reference point to accurately model and predict the mixing and distribution of the fluid in the system. The simulation investigated the influence of flow rate ranging from 10 mg/s to 4,500 mg/s with 50 mg/s intervals. The outlet's findings were shown as quantitative values and a graphical representation of concentration gradients (mol/m^3).

2.4. Fabrication of PDMS microfluidic device

The fabrication of a microfluidic device using a PDMS mixture with silicon began with creating a 3D-printed mold. This mold served as the template for the device and was created using a 3D printer. Next, a mixture of PDMS and silicon was prepared and poured into the mold in a specific ratio of 10:1. After being kept at room temperature for one hour to ensure no visible bubbles; the mixture was baked in a vacuum chamber for 60 minutes at 60 °C. If the combination did not fill the mold correctly or if there were any defects, the process was repeated, starting with creating a new 3D-printed mold. However, if the mixture filled the mold correctly and there were no defects, the process moved on to the final mold step. In this step, the PDMS mixture with silicon was cured and then removed from the 3D-printed mold to form the last microfluidic device, which was ready for use.

2.5. Characterization of alginate and carbon nanotube microfiber

In this study, the stepper motor library in Arduino was utilized to control the output of a stepper motor for liquid purging in a microfluidic device. To calibrate the motor's revolutions per minute (RPM) value for the desired flow rates, a calibration process was conducted by adjusting the step size and manually measuring the RPM. The microfibers were produced by extruding alginate and carbon nanotube solutions through a syringe needle and collecting them in a calcium chloride solution. The properties of the microfibers, including their diameter and conductivity, were characterized and analyzed using statistical methods to evaluate the effects of different concentrations of alginate and carbon nanotubes.

2.5.1. Fourier transform infrared spectroscopy (FTIR)

FTIR was used to examine the structural characteristics of alginate microfibers containing carbon nanotubes and calcium chloride. A PerkinElmer Spectrum 100 FTIR spectrometer with an attenuated total reflectance (ATR) accessory was used to perform the analysis. The sample was placed on an ATR window and

exposed to a mid-IR beam, and the resulting absorption spectrum was recorded over a range of wavelengths. The PerkinElmer Spectrum software was used to analyze the FTIR spectra and identify functional groups such as hydroxyl, carboxyl, and amine groups to confirm the incorporation of the additives. The FTIR spectra were also used to assess the degree of crosslinking and changes in the structural properties of the microfibers after the addition of the carbon nanotubes and calcium chloride.

2.5.2. Raman spectroscopy

Raman spectroscopy was used to analyze the vibrational properties of a mixture of alginate and carbon nanotubes (CNTs) in calcium chloride distilled water. The sample was prepared by homogenizing a known amount of alginate and CNTs with calcium chloride distilled water and then measured using a Raman spectrophotometer. The scattered light was collected and analyzed to obtain the Raman spectrum, which showed peaks corresponding to different vibrational modes of the sample molecules. These peaks were used to identify the other chemical compounds in the sample and study their interactions. Careful control of sample preparation and measurement conditions ensured accuracy and repeatability.

2.5.3. X-ray diffraction

XRD was used to study the structure of alginate-CNT mixed with calcium chloride in distilled water. The resulting mixture was placed on an X-ray diffractometer, and the XRD pattern was obtained by measuring the intensity of the diffracted X-rays as a function of the diffraction angle. The XRD pattern provided information on the crystal structure, crystallinity, and preferred orientation of the sample and how CNTs and calcium chloride affected the design of the alginate. Careful sample preparation and measurement conditions were essential for accuracy and repeatability. The crystallite size was calculated using the formula crystallite size $= k\lambda/(b \cos \theta)$, and the percentage change in crystallite size was calculated using $\{(G_t-G_c)/G_c\}x100$, where Gc and Gt are the relative crystallite sizes of the control and treated powder samples.

3.   RESULTS AND DISCUSSION

In this section, it is explained the results of the research and, at the same time, is given a comprehensive discussion. Results can be presented in figures, graphs, tables, and others that make the reader understand easily [19], [20]. The discussion can be made in several sub-sections.

3.1. The simulation of the microfluidic device's fluid flow and pressure

COMSOL Multiphysics 5.6 was used to model and simulate the microfluidic device on a computer configured: Windows 10 64-bit, 2.4GHz Intel Core i5 CPU, 8GB RAM. As shown in Figure 4, the two-phase flow, level set model, shows that increasing continuous phase velocity reduces droplet size. The concentration gradient graph is generated by COMSOL Multiphysics simulation of fluid dilution and mixing using a microfluidic device to separate and route fluids to the appropriate curved channel at tier. Figure 5 shows the microfluidic device velocity magnitude (m/s) simulation at 0.130 with a log graph (concentration gradient against outlet) and coefficient of determination (R^2). The short flow channel creates flow resistance, allowing fluid to flow to the output channel and creating the curved channels at tiers 1 and 2. Because passive mixing relies solely on molecular diffusion, the curve channel shape helped. Microfluidic efficiency improves as advection is generated at a high flow rate [21]. Diffusion was when molecules move from a high to a low concentration, following the concentration gradient.
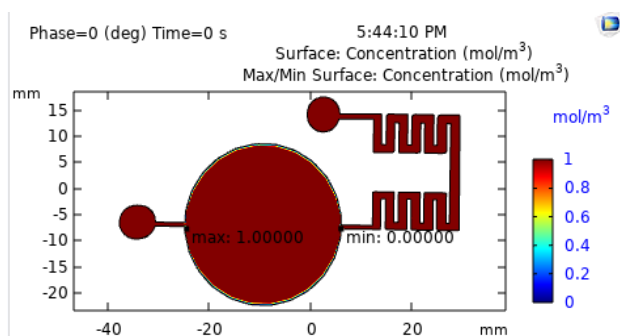

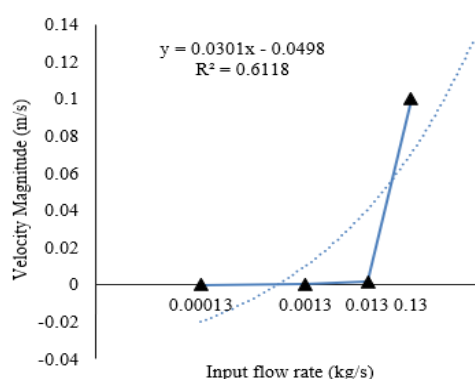Figure 4. The concentration of the microfluidic device in the unit of mol/m³

Figure 5. Simulation result of microfluidic device velocity magnitude

3.2. Characterization of alginate and carbon nanotube
3.2.1. Fourier transform infrared (FTIR) spectroscopy

Figure 6 shows the Fourier transform infrared (FTIR) spectra of the prepared alginate-carbon nanotube and calcium chloride in deionized water, which were measured for various laser pulse energy and repetition rates in the wavenumber range of 1000 to 4,000 cm^{-1}. The relative vibrations of the hydroxyl group (OH) and hydrogen stretching bonds in water molecules were assigned to the FTIR bands that emerged at 3,297 cm^{-1} O-H [22], [23]. The highest peak at around 1,116, 1,424; 1,825, and 2,771 cm^{-1} corresponded to the stretched vibration of C$^-$O and COO$^-$ [24]. The occurrence of the weaker band at 2,238 cm^{-1} band was authorized for C=C stretching mode, whereas the sharp band positioned at 1,636 cm^{-1} was due to C=O stretching mode of the carbonyl group respectively [25], [26]. When the CNTs pretreated with nitric acid were mixed with calcium alginate, a marked increase was spotted in the concentration ratio at around 1,116, 1,424; 1,825, and 2,771 cm^{-1} corresponded to the stretched vibration of C$^-$O and COO$^-$ [21]. In summary, the FTIR spectral analysis confirmed the purity of the alginate-carbon nanotube and calcium chloride, all of which were free of any impurities. All the detected FTIR absorption peaks were attributed to the vibrational bonds of water.

3.2.2. Raman spectroscopy

Raman spectroscopy is an effective method for determining the degree of disorder in CNTs. Expanded studies were implemented between 500 and 3,500 cm^{-1} for the best result. Figure 7 shows the Raman spectroscopy of alginate carbon nanotube powder, and calcium chloride. The highest peak was band D at 1,264 cm^{-1} and band G at 1,498 cm^{-1} [27], [28]. The structural, edge, and dangling effects of disordered band D. The band D or band G intensity ratio (I_D/I_G) is often used to characterize the defect or disordered carbon structure [29], [30]. However, in this study, the intensity ratio (I_D/I_G) was found to be 0.843, attributable to the crystallite's great purity and support for the multilayered graphene [31]. The amount of disorder created in bulk samples was shown by the ratio of the D band to the G band. If both bands are equally intense, the bulk samples contain significant disorder. The relationships between the D band, G band, and RBM are crucial in differentiating between the various CNT variations.
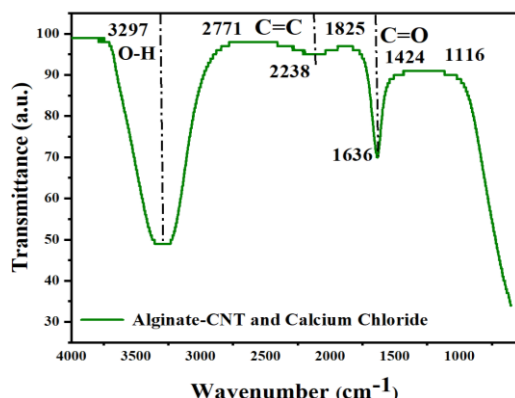

Figure 6. The FTIR spectra of the as-prepared alginate-carbon nanotube and calcium chloride in deionized water
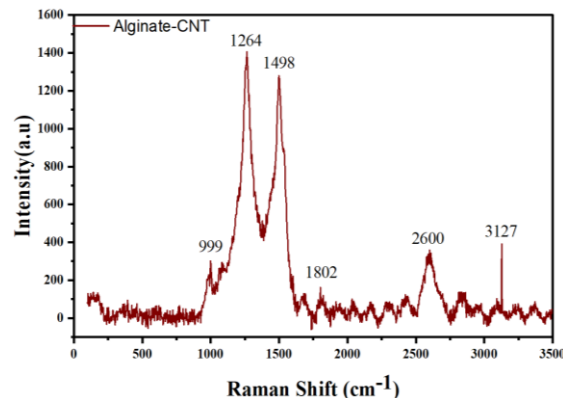
Figure 7. Raman spectroscopy of alginate and carbon nanotube powder and calcium chloride

3.2.3. X-ray diffraction

Figure 8 depicts sodium alginate's X-ray diffraction (XRD) pattern with carbon nanotube and calcium chloride. It was prepared by dipping a piece of a microscope glass slide (25.4×76.2 cm) coated with CNTs and sodium alginate solution into aqueous calcium chloride solution". The peak $2\theta = 26°$, 42, and 44 that can be indexed to (002), (100), and (102) lattice planes of sodium alginate with carbon nanotube and calcium chloride shows an amorphous structure [32]. The X-ray diffraction (XRD) pattern of the sodium alginate with carbon nanotube and calcium chloride as prepared clearly reveals its crystalline structure. The diffraction pattern has a crystallinity index ranging from 30% to 40% and from peak 2θ 51 to 77, respectively.

3.2.4. Field emission scanning electron microscopy (FE-SEM)

Using FESEM, it was possible to characterize the surface morphology, the CNT thin film, and fiber dimensions of the alginate-CNTs and calcium chloride, which were shown in Figures 9 and 10. Additionally, the average diameter of the fiber is extracted from the FESEM image and was depicted in Figure 10 ranges roughly from 16.7 um to 30.5 um. FESEM ensured that CNT films on the substrates have

uniform fiber distribution.

Figure 10 shows the FE-SEM images for determining the diameter and standard deviation of the fibers. It can be seen that the average diameter of the microfiber was 1 (um), as shown in Figure 10. The variation in fiber length with the CNT loading makes it evident that the surface tension, viscosity, and conductivity of the nanocomposite solution impact the fiber length and, consequently, the morphology of the microfibers [33]. Because there was no accumulation and the CNTs were evenly dispersed throughout the PS matrix, this indicated enhanced interfacial compatibility with the polymer chains [34]. The microfiber diameter impacts the membrane's surface roughness and surface energy by increasing the former and decreasing the latter. The membranes' microfiber nature results in developing a fine, networked porous structure, which is very advantageous for the oil/water separation flow [35].

3.2.5. Generated microfibers

Microfluidic devices provide several benefits over conventional devices, including the ability to create fibers with complicated shapes by simply adjusting flow rates, the types of solutions incorporated, and solution concentrations. In particular, the flow rates could be altered by regulating the wettability of microchannels, such as by coating them with hydrophobic or hydrophilic substances.
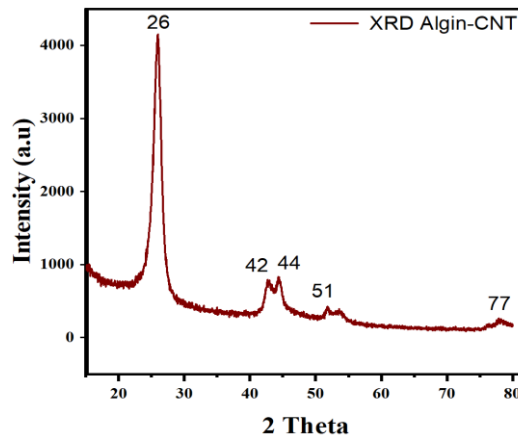

Figure 8. XRD of alginate with carbon nanotube powder and calcium chloride
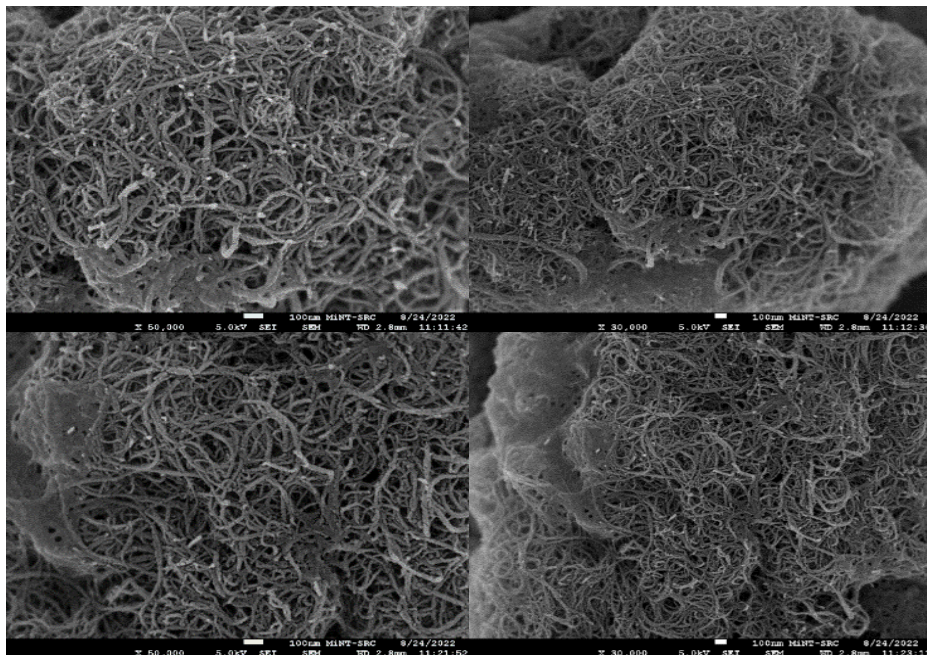

Figure 9. FESEM images for content and nanostructure of alginate-CNT with calcium chloride
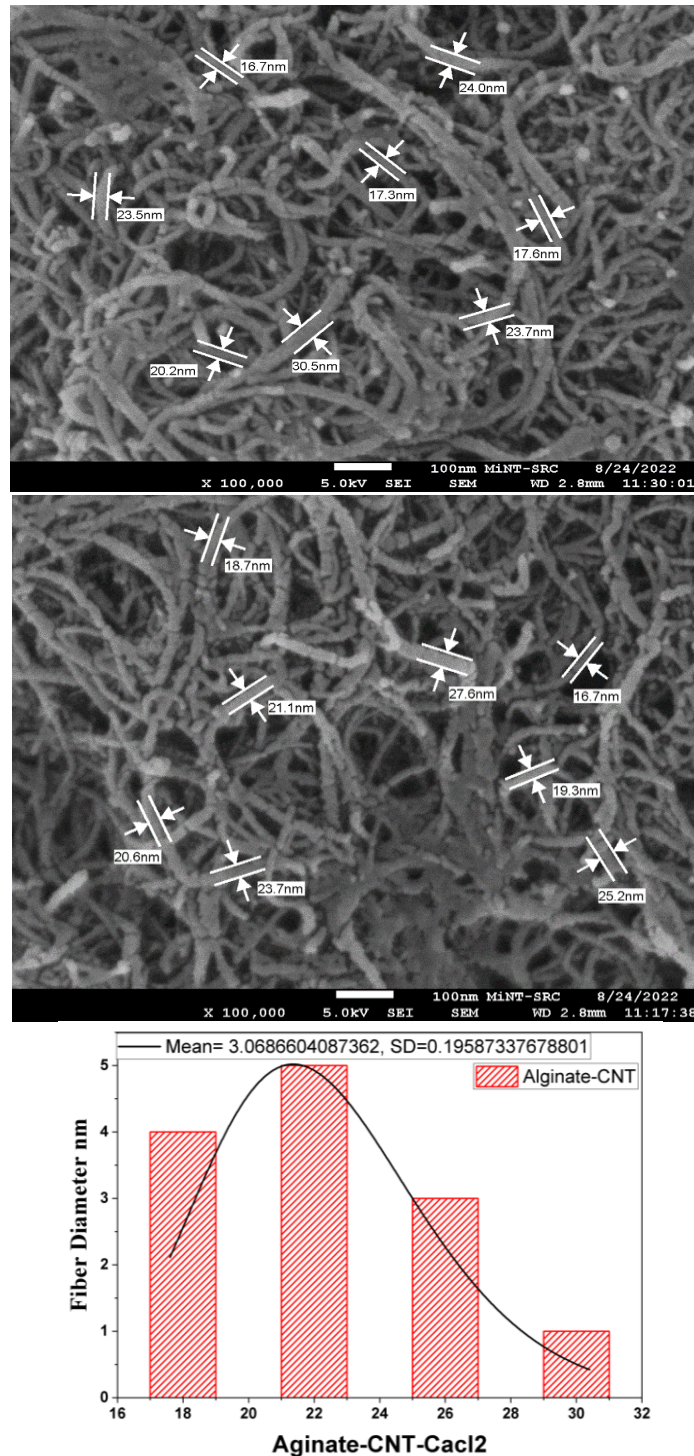
Figure 10. FE-SEM images for determining the diameter and standard deviation of the fibers

Figure 11 shows the alginate-CNT moved from the microfluidic device to inside the calcium chloride to produce the conductive microfibers with different motor speeds. Microfluidic spinning techniques may also manufacture microfibers by a quick chemical crosslinking reaction between the core and sheath solutions. In particular, the polymer precursor solution and the crosslinking agent solution are injected into the core layer and sheath layer, respectively. When the two fluids come into contact, the crosslinking agent monomers permeate into the core layer solution, causing the polymer to crosslink quickly [36]. The alginate-CNT fibers might have diameters between 16.7 um and 30 um as shown in Table 1.

3.2.6. Thickness of the microfibers

After drying, the alginate and carbon nanotube microfibers were printed by an FDM method in various thicknesses with a 1 cm length, as shown in Table 1. To explore the effect of varying alginate and carbon nanotube concentrations (5, 6, and 7%) on the thickness of the alginate and carbon nanotube microfibers, thickness surface analysis was measured using the Image J software step surface profiler. For the thickness side, surface scanning was performed ten times for each sample, and the average value was calculated [37].
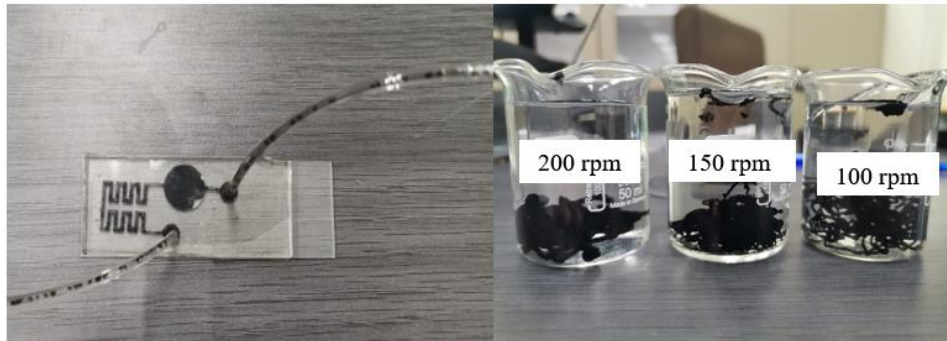
Figure 11. The operation of producing the fibers

Table 1. The generated fibers with different concentrations and motor speeds

The concentrations (%)	The motor speed (RPMs)		
	100	150	200
5%			
6%			
7%			

Figure 12 shows that the specific tensile strengths of CNT microfibers were almost identical for lengths between 0.125 um and 0.275 um merits attention since it suggests that the alginate and CNT microfibers

have a high degree of homogeneity. Additionally, the alginate-CNTs and calcium chloride concentration were primarily within 5%, 6%, and 7% of each other, respectively, and the motor's speed was 100, 150, and 200 rpm. From Figure 12, it can be observed that in 5%, 6%, and 7% concentrations, the microfibers length increased when the alginate and carbon nanotube concentration increased, as the speed rose also. Future generations of high-strength and high-toughness fibers will be made possible by the advancement of continuous preparation technologies and cost reduction.

Figure 13 shows the reference experiment of the I-V characteristic of the alginate and carbon nanotube microfibers. This involved the three speeds of the motor, 100 (rpm), 150 (rpm), and 200 (rpm) in (7%) concentrations of the alginate-CNT and calcium chloride ($CaCl_2$). Most significantly, the curve conforms with Ohm's law quite closely. The slope of the I-V curve goes up, demonstrating decreased resistance, as the concentration of the alginate-CNT solution increased. As the carbon nanotube solution concentration increased, the alginate-CNT microfiber's resistance decreased.
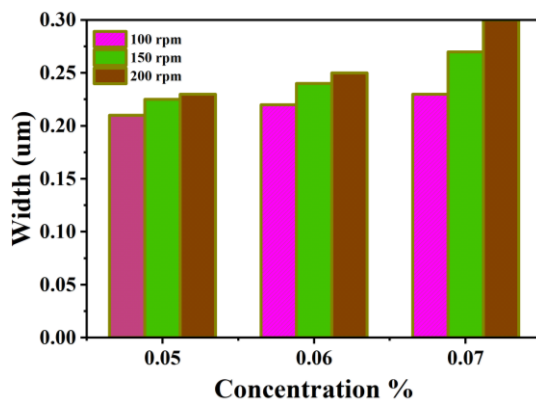

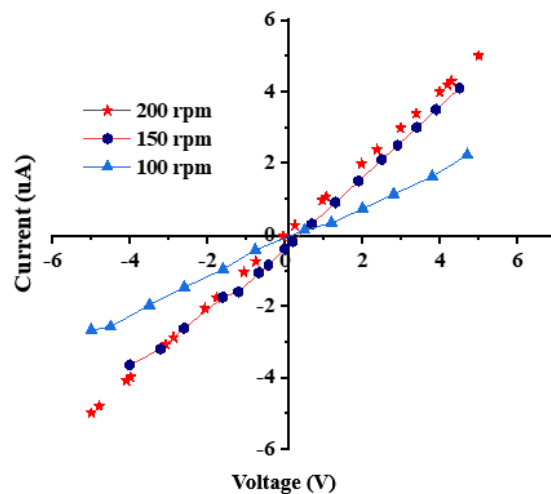Figure 12. The thickness of microfibers

Figure 13. The I-V characteristic of the alginate's carbon nanotube microfibers at 7% solution

4. CONCLUSION

In conclusion, the successful development of a microfluidic device and electronic infusion system has allowed the fabrication of alginate microfibers embedded with carbon nanotubes. The simulation results from COMSOL Multiphysics showed that the device is highly effective in controlling fluid flow and pressure, with optimized values of 2000 um for output width, 100-200 rpm for continuous flow rates, and microfibers ranging from 10 to 100 um in size. The characterization of the microfibers using Fourier transform infrared spectroscopy, Raman spectroscopy, and X-ray diffraction confirmed the successful incorporation of carbon nanotubes and consistent dimensions of the microfibers, which were also observed to exhibit good mechanical stability due to high hydrogen bonding in their chemical composition. I-V characterization showed promising electrical conductivity, indicating potential applications in tissue engineering and drug delivery.

This study highlights the potential of 3D printing technology for the fabrication of functional microfibers, and the results suggest that the microfluidic device and electronic infusion system can be further optimized for higher precision and throughput. Specifically, future work could focus on optimizing the aperture size of the crossed-junction outlet for microfiber production and investigating other potential applications of the resulting microfibers beyond those already mentioned. Overall, this work represents a significant step forward in microfluidics and demonstrates the feasibility of using this technology to produce functional alginate microfibers with embedded carbon nanotubes.

REFERENCES

[1]   Y. H. Yin, "Development of A Microfluidic Device and Electronic Infusion System to Fabricate Microcapsules of Calcium Alginate," M.S. thesis, Faculty of Electrical and Electronic Engineering, University Tun Hussein Onn Malaysia, Parit Raja, Malaysia, 2016, [Online]. Available: https://core.ac.uk/download/pdf/78469317.pdf.

[2]   G. Yang, X. Li, Y. He, J. Ma, G. Ni, and S. Zhou, "From nano to micro to macro: Electrospun hierarchically structured polymeric fibers for biomedical applications," *Progress in Polymer Science*, vol. 81, pp. 80–113, Jun. 2018, doi: 10.1016/j.progpolymsci.2017.12.003.

[3]   B. Huang, "Carbon nanotubes and their polymeric composites: the applications in tissue engineering," *Biomanufacturing Reviews*, vol. 5, no. 3, Dec. 2020, doi: 10.1007/s40898-020-00009-x.

[4]   R. Reddy Eamani, V. Nallathambi, and S. Asaithambi, "A low-power high-speed full adder cell using carbon nanotube field-effect transistors," *Indonesian Journal of Electrical Engineering and Computer Science*, vol. 31, no. 1, pp. 134–142, Jul. 2023, doi: 10.11591/ideas.v31.i1.pp134-142.

[5]   S. Regmi, C. Poudel, R. Adhikari, and K. Q. Luo, "Applications of Microfluidics and Organ-on-a-Chip in Cancer Research," *Biosensors*, vol. 12, no. 7, p. 459, Jun. 2022, doi: 10.3390/bios12070459.

[6]   H. Abu Owida, N. M. Turab, and J. Al-Nabulsi, "Carbon nanomaterials advancements for biomedical applications," *Bulletin of Electrical Engineering and Informatics*, vol. 12, no. 2, pp. 891–901, Apr. 2023, doi: 10.11591/eei.v12i2.4310.

[7]   M. Mohamed Mafroos, H. H. Jameela Sapingi, and A. Hamzah, "Passively Q-switched erbium doped fiber laser based on graphene and carbon nanotube saturable absorbers," *Indonesian Journal of Electrical Engineering and Computer Science*, vol. 28, no. 1, pp. 227–233, Oct. 2022, doi: 10.11591/ijeecs.v28.i1.pp227-233.

[8]   Y. Kurokawa, D. T. Nguyen, R. Fujimoto, and K. Taguchi, "Enhancing DSSC conversion efficiency by ozone-treated TiO2 photoanode and optimum CNT/PDDA counter electrode," *International Journal of Electrical and Computer Engineering (IJECE)*, vol. 10, no. 3, pp. 2926–2933, Jun. 2020, doi: 10.11591/ijece.v10i3.pp2926-2933.

[9]   S. Farhana, "Design of carbon nanotube field effect transistor (CNTFET) small signal model," *International Journal of Electrical and Computer Engineering (IJECE)*, vol. 10, no. 1, pp. 180–187, Feb. 2020, doi: 10.11591/ijece.v10i1.pp180-187.

[10]   A. Dixit and N. Gupta, "Simulations of the CNFETs using different high-k gate dielectrics," *Bulletin of Electrical Engineering and Informatics*, vol. 9, no. 3, pp. 943–949, Jun. 2020, doi: 10.11591/eei.v9i3.1784.

[11]   D. Ji *et al.*, "Smartphone-based differential pulse amperometry system for real-time monitoring of levodopa with carbon nanotubes and gold nanoparticles modified screen-printing electrodes," *Biosensors and Bioelectronics*, vol. 129, pp. 216–223, Mar. 2019, doi: 10.1016/j.bios.2018.09.082.

[12]   A. Nasir, A. Kausar, and A. Younus, "A Review on Preparation, Properties and Applications of Polymeric Nanoparticle-Based Materials," *Polymer-Plastics Technology and Engineering*, vol. 54, no. 4, pp. 325–341, Mar. 2015, doi: 10.1080/03602559.2014.958780.

[13]   Y. Liu, L. Sun, H. Zhang, L. Shang, and Y. Zhao, "Microfluidics for Drug Development: From Synthesis to Evaluation," *Chemical Reviews*, vol. 121, no. 13, pp. 7468–7529, Jul. 2021, doi: 10.1021/acs.chemrev.0c01289.

[14]   H. Fallahi, J. Zhang, H.-P. Phan, and N.-T. Nguyen, "Flexible Microfluidics: Fundamentals, Recent Developments, and Applications," *Micromachines*, vol. 10, no. 12, p. 830, Nov. 2019, doi: 10.3390/mi10120830.

[15]   M. A. Heinrich *et al.*, "3D Bioprinting: from Benches to Translational Applications," *Small*, vol. 15, no. 23, Jun. 2019, doi: 10.1002/smll.201805510.

[16]   J. Guo, Y. Yu, H. Wang, H. Zhang, X. Zhang, and Y. Zhao, "Conductive Polymer Hydrogel Microfibers from Multiflow Microfluidics," *Small*, vol. 15, no. 15, Apr. 2019, doi: 10.1002/smll.201805162.

[17]   M. Guo *et al.*, "Selective laser melting additive manufacturing of pure tungsten: Role of volumetric energy density on densification, microstructure and mechanical properties," *International Journal of Refractory Metals and Hard Materials*, vol. 84, p. 105025, Nov. 2019, doi: 10.1016/j.ijrmhm.2019.105025.

[18]   T. C. Mokhena, M. J. Mochane, A. Mtibe, M. J. John, E. R. Sadiku, and J. S. Sefadi, "Electrospun Alginate Nanofibers Toward Various Applications: A Review," *Materials*, vol. 13, no. 4, p. 934, Feb. 2020, doi: 10.3390/ma13040934.

[19]   A. Mokhberdoran, A. Carvalho, N. Silva, H. Leite, and A. Carrapatoso, "Design and implementation of fast current releasing DC circuit breaker," *Electric Power Systems Research*, vol. 151, pp. 218–232, Oct. 2017, doi: 10.1016/j.epsr.2017.05.032.

[20]   A. Shukla and G. D. Demetriades, "A Survey on Hybrid Circuit-Breaker Topologies," *IEEE Transactions on Power Delivery*, vol. 30, no. 2, pp. 627–641, Apr. 2015, doi: 10.1109/TPWRD.2014.2331696.

[21]   B. Wei, J. Wang, Z. Chen, and G. Chen, "Carbon-Nanotube–Alginate Composite Modified Electrode Fabricated by In Situ Gelation for Capillary Electrophoresis," *Chemistry – A European Journal*, vol. 14, no. 31, pp. 9779–9785, Oct. 2008, doi: 10.1002/chem.200801124.

[22]   K. Fujie, "Boundedness in a fully parabolic chemotaxis system with singular sensitivity," *Journal of Mathematical Analysis and Applications*, vol. 424, no. 1, pp. 675–684, Apr. 2015, doi: 10.1016/j.jmaa.2014.11.045.

[23]   T. Thirunavukkarasu, H. A. Sparkes, C. Balachandran, S. Awale, K. Natarajan, and V. G. Gnanasoundari, "Bis(μ-chloro) bridged 1D Cu I and Cu II coordination polymer complex and mononuclear Cu II complex: Synthesis, crystal structure and biological properties," *Journal of Photochemistry and Photobiology B: Biology*, vol. 181, pp. 59–69, Apr. 2018, doi: 10.1016/j.jphotobiol.2018.02.013.

[24]   L. Fuks, D. Filipiuk, and M. Majdan, "Transition metal complexes with alginate biosorbent," *Journal of Molecular Structure*, vol. 792–793, pp. 104–109, Jul. 2006, doi: 10.1016/j.molstruc.2005.12.053.

[25]   P. C. Nagajyothi, T. V. M. Sreekanth, J. Lee, and K. D. Lee, "Mycosynthesis: Antibacterial, antioxidant and antiproliferative activities of silver nanoparticles synthesized from Inonotus obliquus (Chaga mushroom) extract," *Journal of Photochemistry and Photobiology B: Biology*, vol. 130, pp. 299–304, Jan. 2014, doi: 10.1016/j.jphotobiol.2013.11.022.

[26]   M. Taran, M. Rad, and M. Alavi, "Biological synthesis of copper nanoparticles by using Halomonas elongata IBRC-M 10214," *Industria Textila*, vol. 67, no. 5, pp. 351–356, 2016, [Online]. Available: https://www.researchgate.net/publication/311223512_Biological_synthesis_of_copper_nanoparticles_by_using_Halomonas_elongata_IBRC-M_10214.

[27]   Y. Liu, C. Pan, and J. Wang, "Raman spectra of carbon nanotubes and nanofibers prepared by ethanol flames," *Journal of Materials Science*, vol. 39, pp. 1091–1094, Feb. 2004, doi: 10.1023/B:JMSC.0000012952.20840.09.

[28]   M. Llorens-Gámez and Á. Serrano-Aroca, "Low-Cost Advanced Hydrogels of Calcium Alginate/Carbon Nanofibers with Enhanced

Water Diffusion and Compression Properties," *Polymers*, vol. 10, no. 4, p. 405, Apr. 2018, doi: 10.3390/polym10040405.

[29] A. Jorio and R. Saito, "Raman spectroscopy for carbon nanotube applications," *Journal of Applied Physics*, vol. 129, Jan. 2021, doi: 10.1063/5.0030809.

[30] A. C. Ferrari and J. Robertson, "Interpretation of Raman spectra of disordered and amorphous carbon," *Physical Review B*, vol. 61, no. 20, pp. 14095–14107, May 2000, doi: 10.1103/PhysRevB.61.14095.

[31] L. F. de Paula Santos *et al.*, "The influence of carbon nanotube buckypaper/poly (ether imide) mats on the thermal properties of poly (ether imide) and poly (aryl ether ketone)/carbon fiber laminates," *Diamond and Related Materials*, vol. 116, p. 108421, Jun. 2021, doi: 10.1016/j.diamond.2021.108421.

[32] A. Sarkar and T. Daniels-Race, "Electrophoretic Deposition of Carbon Nanotubes on 3-Amino-Propyl-Triethoxysilane (APTES) Surface Functionalized Silicon Substrates," *Nanomaterials*, vol. 3, no. 2, pp. 272–288, May 2013, doi: 10.3390/nano3020272.

[33] T. Lin, H. Wang, H. Wang, and X. Wang, "The charge effect of cationic surfactants on the elimination of fibre beads in the electrospinning of polystyrene," *Nanotechnology*, vol. 15, no. 9, pp. 1375–1381, Sep. 2004, doi: 10.1088/0957-4484/15/9/044.

[34] J. Peng, Q. Liu, Z. Xu, and J. Masliyah, "Novel Magnetic Demulsifier for Water Removal from Diluted Bitumen Emulsion," *Energy & Fuels*, vol. 26, no. 5, pp. 2705–2710, May 2012, doi: 10.1021/ef2014259.

[35] U. Zulfiqar, A. G. Thomas, A. Matthews, and D. J. Lewis, "Surface Engineering of Ceramic Nanomaterials for Separation of Oil/Water Mixtures," *Frontiers in Chemistry*, vol. 8, Nov. 2020, doi: 10.3389/fchem.2020.00578.

[36] M. Zhang, X. Peng, P. Fan, Y. Zhou, and P. Xiao, "Recent Progress in Preparation and Application of Fibers Using Microfluidic Spinning Technology," *Macromolecular Chemistry and Physics*, vol. 223, no. 5, Mar. 2022, doi: 10.1002/macp.202100451.

[37] M. A. U. Rehman, Q. Chen, A. Braem, M. S. P. Shaffer, and A. R. Boccaccini, "Electrophoretic deposition of carbon nanotubes: recent progress and remaining challenges," *International Materials Reviews*, vol. 66, no. 8, pp. 533–562, Nov. 2021, doi: 10.1080/09506608.2020.1831299.

BIOGRAPHIES OF AUTHORS

Abdulsalam Ali Ahmed Salman was born in Al-Mahweet, Yemen, and received his bachelor's degree in electrical and electronic engineering from Universiti Malaysia Pahang (UMP) in 2020. Currently, he is a master student with research interests of development of microfluidic devices and electronic infusion systems to fabricate microfibers of alginate and carbon nanotubes. He can be contacted at email: alalal4429@gmail.com.

Prof. Madya Ir. Dr. Chin Fhong Soon is a renowned academician and researcher in the field of engineering. She holds a Ph.D. in Chemical Engineering from the University of Bradford, United Kingdom, and is a registered Professional Engineer (P.Eng.) and Chartered Engineer (C.Eng.). Currently, she is a Professor of Chemical Engineering at the Universiti Tun Hussein Onn Malaysia (UTHM), where she has been actively involved in teaching and research for more than 20 years. Her research interests include biomass and bioenergy, renewable energy, and environmental engineering. She has published numerous articles in high-impact journals and has been invited to speak at various international conferences. Additionally, she is an editorial board member of several esteemed journals in her field. Dr. Soon's contributions to the field of engineering have been widely recognized, and she has received numerous awards and honors for her work. She can be contacted at email: soon@uthm.edu.my.

Dr. Gim Pao Lim is a researcher in the field of bioprocess engineering. He holds a Ph.D. in bioprocess engineering from the Universiti Malaysia Perlis. He worked as a postdoctoral at the university Tun Hussein Onn Malaysia for more than 3 years. His research interests include MXene, biopolymers, nanomaterials, and control release studies. He has published numerous articles in high impact journals and has been invited as a reviewer for high impact journal. He can be contacted at email: gplim@uthm.edu.my.